3332 *Chem. Mater.* **2010,** *22,* 3332–3339
DOI:10.1021/cm100391q

CHEMISTRY OF MATERIALS
Article

Structure and Acid Catalysis of Mesoporous $Nb_2O_5 \cdot nH_2O$

Kiyotaka Nakajima,[†] Tsuyoshi Fukui,[†] Hideki Kato,[†] Masaaki Kitano,[†] Junko N. Kondo,[‡] Shigenobu Hayashi,[§] and Michikazu Hara*[,†,⊥]

[†]*Materials and Structures Laboratory Tokyo Institute of Technology, 4259-R3-33, Nagatsuta-cho, Midori-ku, Yokohama 226-8503, Japan,* [‡]*Chemical Resources Laboratory, Tokyo Institute of Technology, 4259-R1-9, Nagatsuta-cho, Midori-ku, Yokohama 226-8503, Japan,* [§]*Research Institute of Instrumentation Frontier, National Institute of Advanced Industrial Science and Technology (AIST), Central 5, 1-1-1 Higashi, Tsukuba 305-8565 Japan, and* [⊥]*Kanagawa Academy of Science and Technology, Sakado 3-2-1, Takatsu-ku, Kawasaki 213-0012, Japan*

Received November 27, 2009. Revised Manuscript Received April 18, 2010

Mesoporous $Nb_2O_5 \cdot nH_2O$ was prepared using amphiphilic block copolymers (L64, P103, and P123) that acted as structure-directing agents. The pore size in the prepared materials increased with increasing molecular weight of the block copolymer at the same weight percentage of ethylene oxide groups in the following order: P123 > P103 > L64. The obtained samples had BET surface areas of 250−350 $m^2\ g^{-1}$ and pore volumes of 0.2−0.4 mL g^{-1}, which are larger than that of bulk $Nb_2O_5 \cdot nH_2O$. Fourier transform-infrared (FT-IR) analysis using CO and pyridine as basic probe molecules indicated no significant differences in the acid strength of the Lewis and Brønsted acid sites among mesoporous, supermicroporous, and bulk $Nb_2O_5 \cdot nH_2O$. Mesoporous $Nb_2O_5 \cdot nH_2O$ exhibits much higher catalytic activity for the hydrolysis of cellobiose than supermicroporous and bulk $Nb_2O_5 \cdot nH_2O$. However, no significant difference was observed between the activity of bulk and mesoporous $Nb_2O_5 \cdot nH_2O$ samples for Friedel−Crafts alkylation. The results suggest that mesopores consisting of hydrophilic niobium oxide are advantageous for hydrophilic reactions, but not hydrophobic reactions.

Introduction

Niobium-based materials are presently of significant interest in heterogeneous catalysis where they are used as catalyst components or are added in small amounts to catalysts.[1−3] Hydrated niobium oxide ($Nb_2O_5 \cdot nH_2O$; niobic acid) possesses both Lewis acid sites and relatively strong Brønsted acid sites on its surface.[3] The stable acidity of $Nb_2O_5 \cdot nH_2O$, even in the presence of water, makes this material attractive for industrial use as a heterogeneous catalyst,[2,3] and is highly important for the establishment of less expensive and environmentally clean processes, particularly for acid-catalyzed reactions. Recently, we have reported the synthesis of supermicroporous $Nb_2O_5 \cdot nH_2O$ using an amphiphilic block copolymer templating route and subsequent acid catalysis reactions.[4,5] Water washing treatment for template removal afforded a highly hydrated supermicroporous material suitable for acid catalysis. Although the activity of this material is lower than that of $Nb_2O_5 \cdot nH_2O$ for acid-catalyzed reactions in the liquid phase, it does exhibit high catalytic performance for gas-phase esterification and dehydration reactions. The low catalytic activity of supermicroporous $Nb_2O_5 \cdot nH_2O$ in liquid-phase reactions is attributed to the limitations placed on reactant molecule diffusion because of the restricted size of the nanopores (ca. 1.5 nm).[5] Therefore, porous $Nb_2O_5 \cdot nH_2O$ with large pore size could function as a heterogeneous catalyst for various acid-catalyzed reactions.

The synthesis of mesoporous transition metal oxides, including supermicroporous $Nb_2O_5 \cdot nH_2O$, relies on a supramolecular templating mechanism where the assembly of amphiphilic molecules (surfactants) functions as a structure-directing template.[4−8] Mesoporous materials with larger pore sizes could be synthesized using ABA-type amphiphilic block copolymers consisting of a central propylene oxide (PO: $-CH_2CH(CH_3)O-$) block (hydrophobic moiety) sandwiched by two ethylene oxide (EO: $-CH_2CH_2O-$) blocks (hydrophilic moiety).[6−10] In the case of mesoporous silica SBA-15 synthesis,[9,10] the pore diameter and mesoporous structure can be tuned by changing the molecular weight and the EO/PO ratio of

*Corresponding author. Tel: +81-45-924-5381. Fax: +81-45-924-5381. E-mail: mhara@msl.titech.ac.jp.

(1) Nowak, I.; Ziolek, M. *Chem. Rev.* **1999**, *99*, 3603.
(2) Tanabe, K.; Okazaki, S. *Appl. Catal., A* **1995**, *133*, 191.
(3) Tanabe, K. *Catal. Today* **2003**, *78*, 65.
(4) Lee, B.; Lu, D.; Kondo, J. N.; Domen, K. *Chem. Lett.* **2002**, *31*, 1058.
(5) Hiyoshi, M.; Lee, B.; Lu, D.; Hara, M.; Kondo, J. N.; Domen, K. *Catal. Lett.* **2004**, *98*, 181.
(6) Yang, P.; Zhao, D.; Margolese, D. I.; Chmelka, B. F.; Stucky, G. D. *Nature* **1998**, *396*, 152.
(7) Yang, P.; Zhao, D.; Margolese, D. I.; Chmelka, B. F.; Stucky, G. D. *Chem. Mater.* **1999**, *11*, 2813.
(8) Schüth, F. *Chem. Mater.* **2001**, *13*, 3184.
(9) Zhao, D.; Feng, J.; Huo, Q.; Melosh, N.; Fredrickson, H. G.; Chmelka, B. F.; Stucky, G. D. *Science* **1998**, *279*, 548.
(10) Zhao, D.; Huo, Q.; Freng, J.; Chmelka, B. F.; Stucky, G. D. *J. Am. Chem. Soc.* **1998**, *120*, 6024.

Published on Web 05/07/2010

the block copolymers.[11,12] The preparation of ordered mesoporous niobium oxides has been reported using amphiphilic block copolymers as structure-directing agents.[6−8,13−15] Highly ordered mesoporous structure can be formed by the calcination of surfactant-containing precursor under mild conditions. However, despite their large surface areas and pore volumes, these niobium oxides cannot function as solid acids for acid-catalyzed reactions, because the intrinsic Brønsted and Lewis acidity of amorphous niobium oxide is completely removed by the calcination treatment.[2,3] Antonelli et al. reported the preparation of mesoporous niobium oxide with wormhole-like mesopores by the ligand-assisted templating method using an alkylamine surfactant.[16,17] The introduction of strong Brønsted acid sites onto the amorphous niobium framework was successfully achieved by treatment of the material with dilute H_2SO_4 or H_3PO_4 solution.[18] Although the sulfated mesoporous niobium oxide showed higher catalytic activity for the Friedel−Crafts benzylation of anisole and toluene with benzyl alcohol than the corresponding bulk catalyst, severe leaching of sulfur species as active sites with an accompanying decrease in the surface area resulted in significant deactivation of the catalyst.[18] As a result, mesoporous niobium oxide possessing Brønsted and Lewis acid sites such as $Nb_2O_5 \cdot nH_2O$ has not yet been synthesized. Recently, Tagusagawa et al. reported that mesoporous niobium−tungsten mixed oxide (W/Nb = 3/7) can function as a recyclable and highly active solid acid catalyst for esterification, hydrolysis, and Friedel−Crafts alkylation.[19] High catalytic performance in the material is mainly attributed to the high surface area, mesoporous structure, and strongly acidic Brønsted acid sites ($-12 \leq H_0 < 6.6$) formed by Nb^{5+} and W^{6+} ions.

In this study, the synthesis and acid catalysis of mesoporous $Nb_2O_5 \cdot nH_2O$ were studied for potential application to highly efficient acid-catalyzed reactions. Three Pluronic block copolymers (L64, P103, and P123) were adopted for the synthesis of mesoporous $Nb_2O_5 \cdot nH_2O$. Whereas the EO and PO blocks in these polymers comprise the same or approximately the same weight percentage (ca. 34−40 and 60−66 wt %, respectively), they have distinct molecular weights and chain lengths.

Experimental Section

Preparation of Mesoporous and Supermicroporous $Nb_2O_5 \cdot nH_2O$. Amphiphilic block copolymers (L64, P85, P103, and P123) consisting of EO and PO blocks with different chain lengths were adopted as structure-directing agents for the preparation of mesoporous and supermicroporous $Nb_2O_5 \cdot nH_2O$. In a typical synthesis, 7 mmol of niobium(V) chloride and 1.0 mL of 0.05 M NaCl aqueous solution were added to a solution of 10 g of dehydrated 1-propanol containing 1.0 g of amphiphilic block copolymer. After being stirred for 60 min, the sol solution was aged at 313 K in air for 7 days to obtain template-containing niobium oxide. The gel samples were further aged at 473 K for 2 days to consolidate the inorganic framework. Porous $Nb_2O_5 \cdot nH_2O$ samples were obtained by the removal of the template from the aged gel by solvent-extraction treatment. The dry gels were warmed in 300 mL of H_2O at 333 K for 3 h and then filtered. After this treatment was repeated four times, the washed samples were dried in air overnight at 373 K. The resulting materials prepared with L64, P85, P103, and P123 are denoted as $Nb_2O_5 \cdot nH_2O$-L64, $Nb_2O_5 \cdot nH_2O$−P85, $Nb_2O_5 \cdot nH_2O$−P103, and $Nb_2O_5 \cdot nH_2O$−P123, respectively.

Characterization. Structural information of the prepared samples was obtained by scanning electron microscopy (SEM; S-5200, Hitachi), N_2 adsorption analysis (NOVA-4200e, Quantachrome), powder X-ray diffraction (XRD; ULTIMA IV, Rigaku), Fourier transform-infrared spectroscopy (FT-IR; FT/IR-6100, Jasco), and ^{31}P magic angle spinning nuclear magnetic resonance (MAS NMR; ASX400, Bruker). SEM images were obtained using an ultrahigh-resolution SEM system without metal deposition on the samples. Nitrogen adsorption−desorption isotherms were measured at 77 K. Prior to measurement, the samples were pretreated at 423 K for 3 h under vacuum. The Brunauer−Emmett−Teller (BET) surface areas were estimated over a relative pressure (P/P_0) range of 0.05−0.30. Pore size distributions were obtained from analysis of the adsorption branch of the isotherms using the Barrett−Joyner−Halenda (BJH) method. The amount of Brønsted acid sites was estimated by titration with n-butylamine. Samples suspended in benzene solution containing benzalacetophenone as a Hammett indicator ($H_o \leq -5.6$) were titrated by against *n*-butylamine/benzene solution.[20]

The acid properties of the prepared samples were examined using FT-IR. FT-IR spectra were obtained at a resolution of 4 cm^{-1} using a spectrometer equipped with an extended KBr beam splitting device and a mercury cadmium telluride (MCT) detector. A total of 64 scans were averaged for each spectrum. $Nb_2O_5 \cdot nH_2O$ samples were pressed into self-supporting disks (20 mm diameter, 20−30 mg) and placed in an IR cell attached to a closed circulation system. The sample was dehydrated by heating the self-supported disk at 423 K for 1 h under a vacuum in order to remove physisorbed water. CO adsorption was investigated by cooling the IR cell with liquid N_2 and introduction of a certain amount of CO into the IR cell at 90 K. The IR spectrum of the dehydrated sample at 90 K was used as a background. Background-subtracted IR spectra showing adsorbed species are presented throughout this paper. For pyridine adsorption, the IR spectrum of a dehydrated sample (423 K for 1 h under vacuum) at room temperature was used as the background spectrum and a certain amount of pyridine was introduced into the IR cell at room temperature.

(11) Kipkemboi, P.; Fogden, A.; Alfredsson, V.; Flodstom, K. *Langmuir* **2001**, *17*, 5398.
(12) Nowak, I.; Ziolek, M.; Jaroniec, M. *J. Phys. Chem. B* **2004**, *108*, 3722.
(13) Tian, B.; Liu, X.; Tu, B.; Yu, C.; Fan, J.; Wang, L.; Xie, S.; Stucky, G. D.; Zhao, D. *Nat. Mater.* **2003**, *2*, 159.
(14) Xu, X.; Tian, B.; Zhang, S.; Kong, J.; Zhao, D.; Liu, B. *Anal. Chim., Acta* **2004**, *519*, 31.
(15) Lee, B.; Lu, D.; Kondo, J. N.; Domen, K. *J. Am. Chem. Soc.* **2002**, *124*, 11256.
(16) Antonelli, D. M.; Ying, J. Y. *Angew. Chem., Int. Ed.* **1996**, *35*, 426.
(17) Antonelli, D. M.; Nakahira, A.; Ying, J. Y. *Inorg. Chem.* **1996**, *35*, 3126.
(18) Rao, Y.; Trudeau, M.; Antonelli, D. *J. Am. Chem. Soc.* **2006**, *128*, 13996.
(19) Tagusagawa, C.; Takagaki, A.; Iguchi, A.; Takanabe, K.; Kondo, N. J.; Ebitani, K.; Hayashi, S.; Tatsumi, T.; Domen, K. *Angew. Chem., Int. Ed.* **2010**, *49*, 1128.
(20) Tanabe, K.; Misono, M.; Ono, Y.; Hattori, H. *New Solid Acids and Bases*; Kodansya Ltd. and Elsevier Science: Tokyo and Amsterdam, 1989.

Table 1. Structural Parameters for the Pluronic-Type Block Copolymers Used in the Synthesis of Mesoporous and Supermicroporous $Nb_2O_5 \cdot nH_2O$

Pluronic	physical form	mol wt (g mol^{-1})	PO length	EO length	PO weight (wt %)	EO weight (wt %)
L64	liquid	2900	30	13	60	40
P103	waxy solid	4950	56	17	66	34
P123	waxy solid	5800	70	20	60	40
P85	waxy solid	4500	39	26	50	50

The acid strength of the materials was also characterized by ^{31}P MAS NMR. Trimethylphosphine oxide (TMPO)-adsorbed samples were prepared in the liquid phase.[21] Two-tenths of a gram samples were dehydrated by evacuation at 423 K for 1 h and soaked in a tetrahydrofuran (THF) solution containing an adequate amount of TMPO at room temperature for 2 days under an Ar atmosphere. After 2 days, TMPO-adsorbed samples were obtained by removal of the THF solvent under vacuum and then packed into a rotor under a N_2 atmosphere. ^{31}P MAS NMR spectra of the TMPO-adsorbed samples were measured at room temperature at a Larmor frequency of 162.0 MHz using a single-pulse sequence with high-power proton decoupling. A Bruker MAS probehead was used with a 4 mm zirconia rotor. The spinning rate of the sample was 8 kHz. The ^{31}P chemical shift was referenced to 85% H_3PO_4 at 0.0 ppm. $(NH_4)_2HPO_4$ was used as a second experimental reference material with the signal set at 1.33 ppm.

Acid-Catalyzed Reaction. The acid catalytic performance was demonstrated through the hydrolysis of cellobiose (373 K) and the Friedel−Crafts alkylation of toluene with benzyl chloride (353 K). For comparison, the catalytic performance of bulk niobic acid (HY-340, CBMM Co.), Nafion-NR50 (Aldrich), Nafion-SAC13 (Aldrich), and Amberlyst-15 (Aldrich) were also examined. Hydrolysis of cellobiose was carried out in a 10 mL aqueous solution containing 0.2 g of cellobiose. Two-tenths of a gram of each catalyst was used in the reactions without pretreatment. Samples were withdrawn from the reaction mixtures at 1 h intervals and analyzed using a high-performance liquid chromatography (HPLC; LC-2000 plus, Jasco) equipped with an Aminex HPX-87H column (BioRad Laboratories). Friedel−Crafts alkylation of toluene with benzyl chloride was performed in a mixture of 100 mmol toluene and 20 mmol benzyl chloride in the presence of 0.2 g of catalyst. Samples were withdrawn from the reaction mixtures at 15 min intervals and analyzed using a gas chromatograph equipped with a capillary column (DD-FFAP, Shimadzu).

Results and Discussion

1. Structural Characterization of Mesoporous $Nb_2O_5 \cdot nH_2O$. Table 1 lists the structural parameters of the Pluronic-type block copolymers used in this study. For the synthesis of mesoporous silica, SBA-15, it has been reported that short EO chain polymers (EO ≤ 4) give rise to a lamellar structure, and a two-dimensional hexagonal (*p6m*) structure is formed with medium chain polymers (17 ≤ EO ≤ 37).[11] On the other hand, long chain polymers (ca. 132 ≤ EO) result in a cubic structure.[11] Structural information for the prepared samples was investigated by XRD analysis. Figure 1 shows XRD patterns of the prepared $Nb_2O_5 \cdot nH_2O$ (A) before and (B) after surfactant extraction. The XRD profiles for the as-prepared samples in Figure 1(A) display a strong intensity signal at

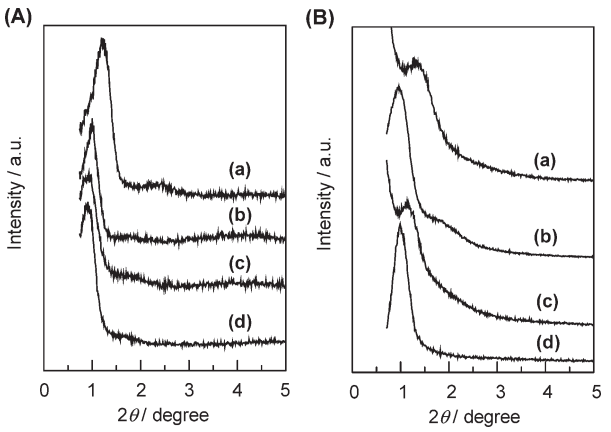

Figure 1. XRD patterns for supermicroporous and mesoporous $Nb_2O_5 \cdot nH_2O$ (A) before and (B) after template extraction. (a) L64, (b) P85, (c) P103, and (d) P123 were used as structure-directing agents.

1.0−1.5° with a weak signal at 1.5−2.5°. These patterns are typical for mesoporous solids synthesized using neutral surfactants,[22,23] which indicaties that these copolymers also act as structure-directing agents for mesoporous $Nb_2O_5 \cdot nH_2O$. These XRD profiles are similar to that of HMS with wormhole-like mesoporous structure.[22] The intense diffraction shifts to lower 2θ with increase in the PO chain length, which suggests that the repeat distance of the periodic mesoporous structure is directly affected by the PO chain length. After removal of the surfactant by solvent-extraction treatment, dependence of the periodic structure on the surfactant is not observed, as shown in Figure 1(B). Incomplete condensation of the niobium oxide framework is expected in the as-synthesized samples before removal of the surfactant under the present synthesis conditions. Hydrolysis and/or further polycondensation during surfactant removal results in partial degradation of the mesoporous structure. It should be noted that $Nb_2O_5 \cdot nH_2O$−L64 has a larger pore size than $Nb_2O_5 \cdot nH_2O$−P85, although the PO chain length of L64 is shorter than that of P85. This may be attributed to a difference in the partial degradation of the mesoporous structure during surfactant removal.

Figure 2 shows (A) N_2 adsorption−desorption isotherms and (B) BJH pore size distribution curves for porous $Nb_2O_5 \cdot nH_2O$ after surfactant removal. The isotherm for $Nb_2O_5 \cdot nH_2O$−P85 (Figure 2(A)(b)) is in good agreement with that previously reported for supermicroporous niobium oxide, and the average pore size is ca. 1.6 nm.[5] The isotherms for $Nb_2O_5 \cdot nH_2O$−L64, −P103, and −P123 (Figure 2(A)(a),(c), and (d)) show typical type-IV patterns with an almost H1-type hysteresis loop,

(21) Baltusis, L.; Frye, J. S.; Maciel, G. E. *J. Am. Chem. Soc.* **1987**, *109*, 40.
(22) Prouzet, E.; Pinnavaia, T. J. *Angew. Chem., Int. Ed.* **1997**, *36*, 516.
(23) Kim, S.-S.; Pauly, T. R.; Pinnavaia, T. J. *Chem. Commun.* **2000**, 835.

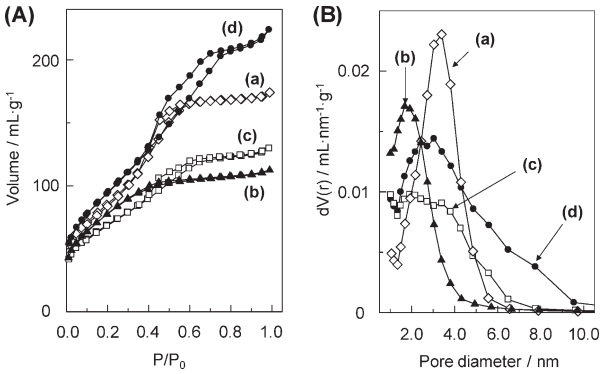

Figure 2. (A) N_2 adsorption−desorption isotherms and (B) BJH pore size distribution curves for supermicroporous and mesoporous $Nb_2O_5 \cdot nH_2O$. (a) L64, (b) P85, (c) P103, and (d) P123 were used as structure-directing agents.

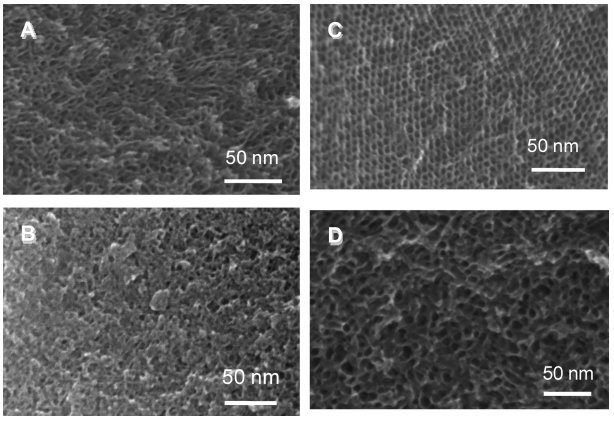

Figure 3. High-resolution SEM images for supermicroporous/mesoporous $Nb_2O_5 \cdot nH_2O$. (A) L64, (B) P85, (C) P103, and (D) P123 were used as structure-directing agents.

which is characteristic of mesoporous materials with cylindrical pores.[24] The sharp N_2 uptake over a narrow range ($P/P_0 = 0.4-0.6$) of the adsorption isotherm for $Nb_2O_5 \cdot nH_2O$−L64 (Figure 1(A)(a)) indicates uniform mesopores (3.4 nm) with a narrow size range in the corresponding pore size distribution curve (Figure 2(B)(a)). On the other hand, the gradual N_2 uptake over a wide range ($P/P_0 = 0.4-0.8$) observed in Figures 2(A)(c) and (d) implies that these samples have broad pore size distribution curves (1.5−10.0 nm), as shown in Figures 2(B)(c) and (d). These results indicate that the pore size distribution of the $Nb_2O_5 \cdot nH_2O$ samples can be tuned by changing the chain length of the amphiphilic block copolymer surfactant; $Nb_2O_5 \cdot nH_2O$−L64 and −P85 have a uniformly sized mesoporous and supermicroporous systems, and $Nb_2O_5 \cdot nH_2O$−P103 and −P123 have both mesoporous and supermicroporous structures. Figure 3 shows high-resolution SEM images of the mesoporous $Nb_2O_5 \cdot nH_2O$ samples. Mesopores are not observed in $Nb_2O_5 \cdot nH_2O$−P85, but are present in the $Nb_2O_5 \cdot nH_2O$−L64, −P103, and −P123 samples, which is consistent with the N_2 adsorption−desorption isotherms and pore size distribution curves. The SEM images in Figures 3(A) and 3(D) show the wormhole-like mesoporous structure in $Nb_2O_5 \cdot nH_2O$−L64 and −P123. While an ordered structure was partially observed in the SEM image for $Nb_2O_5 \cdot nH_2O$−P103 (Figure 3(C)), no long-range hexagonal ordered structure was observed in the sample. Thus, $Nb_2O_5 \cdot nH_2O$−P103 is expected to have a wormhole-like structure. The BET surface area, pore volume, and pore size of the prepared samples are summarized together with the structural parameters of the surfactants in Table 2. The prepared materials have BET surface areas of 250−350 $m^2\,g^{-1}$ and pore volumes of 0.2−0.4 mL g^{-1}, which are larger than that of bulk $Nb_2O_5 \cdot nH_2O$. The amounts of carbon in the samples before and after removal of the templates were estimated to be ca. 24−26 wt % and < 1 wt %, respectively. The amounts were determined by elemental analysis based on combustion and indicated that most of surfactants in these samples could be removed by water-washing. This was not derived from the strong electrostatic interaction, but to relatively weak hydrogen-bonding interaction between the amphiphilic block copolymer surfactant and the hydrated niobium framework.[6,9,10]

2. Characterization of Acid Properties by FT-IR and ^{31}P MAS NMR. FT-IR spectroscopy of probe molecules adsorbed on solid acid catalysts is an effective method for understanding the active sites of the catalysts.[25] Pyridine, carbon monoxide (CO), or ammonia are the most widely known probe molecules for the characterization of acidity.[25−31] Here, CO was used as a weak basic probe molecule for the characterization of both Brønsted and Lewis acid sites.[25,29−31] CO has much lower basicity than pyridine; therefore, the surface Brønsted acid sites do not bind to the protonated pyridines, but bind to CO by hydrogen bonding.[27]

Differential spectra of dehydrated $Nb_2O_5 \cdot nH_2O$−L64, before and after successive doses of CO at 90 K, are displayed in Figure 4. The intensity of the band at ca. 2190 cm^{-1}, which is assignable to ν(CO) from CO adsorbed on the Lewis acid sites,[25] increased with increasing CO pressure. After increasing the CO pressure from 0.3 to 7.0 Torr, three positive peaks at 3500, 2164, and 2144 cm^{-1} and a negative peak at 3704 cm^{-1} appeared simultaneously and were assignable to ν(OH) of the acidic OH groups interacted with CO, ν(CO) from CO adsorbed on the Brønsted acid sites, ν(CO) of physisorbed CO, and ν(OH) of the original acidic OH sites, respectively.[25] The wavenumbers for ν(CO) from CO adsorbed on Lewis acid (ν(CO):LAS, ca. 2190 cm^{-1}) and Brønsted acid (ν(CO):BAS, ca. 2170 cm^{-1}) sites for each of the tested samples are summarized in Table 3. The ν(CO) position has been reported to depend on the acid strength of the acid sites; ν(CO) for stronger acid sites appears at larger wavenumber.[25] There was no significant difference in the wavenumber for ν(CO) among the tested porous and bulk $Nb_2O_5 \cdot nH_2O$ samples, which indicates that there is no

(24) Kruk, M.; Jaroniec, M. *Chem. Mater.* **2001**, *13*, 3169.
(25) Busca, G. *Phys. Chem. Chem. Phys.* **1999**, *1*, 723.
(26) Parry, E. P. *J. Catal.* **1963**, *2*, 371.
(27) Ward, J. W. *J. Catal.* **1967**, *9*, 225.
(28) Sayed, M. B.; Kydd, K. A.; Cooney, R. P. *J. Catal.* **1984**, *88*, 137.
(29) Echoufi, N.; Gelin, P. *J. Chem. Soc., Faraday Trans.* **1992**, *88*, 1067.
(30) Zecchina, A.; Bordiga, S.; Spoto, G.; Scarano, D.; Petrini, G.; Leofanti, G.; Padovan, M.; Arean, C. O. *J. Chem. Soc., Faraday Trans.* **1992**, *88*, 2959.
(31) Hadjiivanov, K. I.; Vayssilov, G. N. *Adv. Catal.* **2002**, *47*, 307.

Table 2. Physicochemical Properties of Supermicroporous, Mesoporous, and bulk $Nb_2O_5 \cdot nH_2O$

	surfactant[a]	S_{BET}[b] ($m^2\ g^{-1}$)	pore volume (mL g^{-1})	pore size (nm)	d (100)-as[c] (nm)	d (100) [d] (nm)
porous $Nb_2O_5 \cdot nH_2O$	L64	312	0.28	3.4	7.4	6.3
	P85	278	0.19	1.6	8.8	9.0
	P103	246	0.21	1.8−8.0	9.5	7.6
	P123	343	0.37	2.0−10.0	10.5	8.9
bulk $Nb_2O_5 \cdot nH_2O$		171	0.09			

[a] Amphiphilic block copolymer consisting of ethylene oxide ($-CH_2CH_2O-$) and propylene oxide ($-CH_2CH(CH_3)O-$) blocks. [b] Estimated over a relative pressure (P/P_0) range of 0.05−0.30. [c] As-made samples. [d] Surfactant-extracted samples.

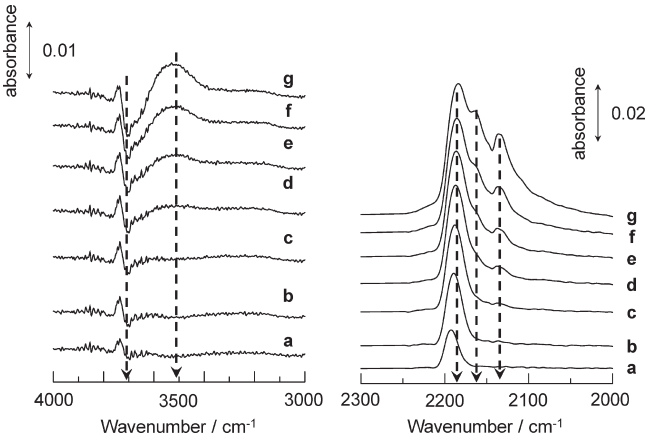

Figure 4. Differential FT-IR spectra for CO-adsorbed $Nb_2O_5 \cdot nH_2O$ prepared with L64. CO pressure: (a) 0.05, (b) 0.10, (c) 0.30, (d) 0.75, (e) 1.4, (f) 3.0, and (g) 7.0 Torr.

Table 3. CO Adsorption Results for Supermicroporous, Mesoporous, And Bulk $Nb_2O_5 \cdot nH_2O$

	surfactant	ν(CO): LAS (cm^{-1})	ν(CO): BAS (cm^{-1})
porous $Nb_2O_5 \cdot nH_2O$	L64	2188	2168
	P85	2189	2166
	P103	2188	2167
	P123	2185	2166
bulk $Nb_2O_5 \cdot nH_2O$		2188	2168

considerable difference in the acidity of the Lewis and Brønsted acid sites among the samples.

The acid strength of the Brønsted acid sites of the solid catalysts was also evaluated using ^{31}P MAS NMR for samples treated with TMPO as a basic probe molecule.[21] The amount of adsorbed TMPO was adjusted to half that of the amount of the Brønsted acid sites on each sample. The peak position of TMPO adsorbed on a Brønsted acid site is downshifted and the degree of peak shift is directly dependent on the acid strength of the catalyst.[21] ^{31}P MAS NMR spectra of bulk $Nb_2O_5 \cdot nH_2O$ and the prepared samples are displayed in Figure 5. One intense signal at 60−70 ppm is clearly observed in all spectra and is assignable to TMPO adsorbed on Brønsted acid sites, which suggests that there is no significant difference in the acid strength of Brønsted acid sites among the prepared samples. This result is in good agreement with that obtained from the FT-IR measurements. In Figure 5c for $Nb_2O_5 \cdot nH_2O$−P103, a resonance peak appears at ca. 40 ppm in addition to the peak due to TMPO-adsorbed Brønsted acid sites. It has been reported that physisorbed TMPO that is not adsorbed by active Brønsted acid sites

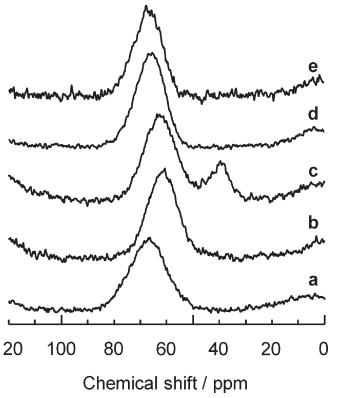

Figure 5. ^{31}P MAS NMR spectra for (a) $Nb_2O_5 \cdot nH_2O$−L64, (b) $Nb_2O_5 \cdot nH_2O$−P85, (c) $Nb_2O_5 \cdot nH_2O$−P103, (d) $Nb_2O_5 \cdot nH_2O$−P123, and (e) bulk $Nb_2O_5 \cdot nH_2O$ after TMPO adsorption. The Brønsted acid/TMPO ratio of the samples was 2.

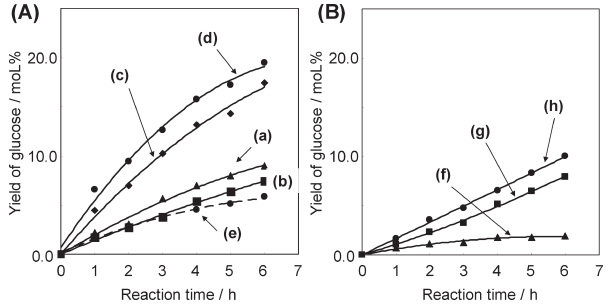

Figure 6. Time courses for D-glucose formation by the hydrolysis of cellobiose over (A) bulk and supermicroporous/mesoporous $Nb_2O_5 \cdot nH_2O$, and (B) strongly acidic resin. (a) Mesoporous $Nb_2O_5 \cdot nH_2O$ prepared with L64, (b) supermicroporous $Nb_2O_5 \cdot nH_2O$ prepared with P85, (c) mesoporous $Nb_2O_5 \cdot nH_2O$ prepared with P103, (d) mesoporous $Nb_2O_5 \cdot nH_2O$ prepared with P123, (e) bulk $Nb_2O_5 \cdot nH_2O$, (f) Nafion-silica (SAC-13), (g) Nafion resin (NR-50), and (h) Amberlyst-15.

aggregates on the solid surface, resulting in a resonance peak at ca. 40 ppm in the ^{31}P MAS NMR spectrum of Figure 5c.[21] This means that a part of TMPO is not adsorbed on the Brønsted acid sites and aggregates on $Nb_2O_5 \cdot nH_2O$−P103 although the amount of TMPO introduced is only half that of the Brønsted acid sites. While the amounts of the Brønsted acid sites (0.1 mmol g^{-1}, see Table 5) and adsorbed TMPO (0.01 mmol TMPO/0.2 g sample) on $Nb_2O_5 \cdot nH_2O$-L64 is the same as that for $Nb_2O_5 \cdot nH_2O$−P103, the peak due to aggregated TMPO is not observed in the former. The minimum pore size (1.8 nm) of the latter is much smaller than that of the former (3.4 nm). This suggests that the narrow mesopores in $Nb_2O_5 \cdot nH_2O$−P103 prevent TMPO from approaching the Brønsted acid sites, which results in the aggregation of a part of the TMPO on the external surface.

Table 4. Catalytic Activity for the Hydrolysis of Cellobiose and Structural Parameters for Supermicroporous, Mesoporous, and Bulk $Nb_2O_5 \cdot nH_2O$, in Addition to Reference Catalysts

	surfactant	acid amount (BAS)[a] (mmoL g^{-1})	S_{BET} (m^2 g^{-1})	pore size (nm)	glucose yield[b] (%)	TOF[c] (h^{-1})
porous $Nb_2O_5 \cdot nH_2O$	L64	0.1	312	3.4	9.0	0.44
	P85	0.4	278	1.6	7.4	0.09
	P103	0.1	246	1.8−8.0	17.4	0.85
	P123	0.7	343	2.0−10.0	19.5	0.14
bulk $Nb_2O_5 \cdot nH_2O$		0.3	171		5.8	0.09
Nafion (NR50)		0.90	< 1		8.0	0.04
Nafion (SAC-13)		0.13	344		1.9	0.07
Amberlyst-15		4.90	50		10.0	0.01

[a] The amount of Brønsted acid sites was estimated by titration with *n*-butylamine. [b] Reaction time 6 h. [c] Reaction time 6 h.

3. Acid Catalysis of Bulk, Supermicroporous, and Mesoporous $Nb_2O_5 \cdot nH_2O$. The catalytic performance of mesoporous and supermicroporous $Nb_2O_5 \cdot nH_2O$ was examined by the hydrolysis of cellobiose (373 K) and Friedel−Crafts alkylation of toluene with benzyl chloride (353 K). Cellobiose is a β-1,4-glucan that consists of two glucose molecules linked by a β-1,4-glycosidic bond, as is cellulose, which is composed of many glucose molecules linked by β-1,4-glycosidic bonds. The hydrolysis of β-1,4-glucan into glucose is an attractive reaction, because glucose can be further converted into industrially important chemicals, including ethanol.[32−34] Nafion resin (NR50),[36] Nafion-silica composite (SAC-13),[37,38] and Amberlyst-15,[36] which are strong polymer-based solid acids with high densities of SO_3H and very high activity for a variety of reactions,[36−38] were used as reference catalysts for comparison. Figure 6(A) and 6(B) shows time courses of the glucose yield from hydrolysis of cellobiose at 373 K. Bulk $Nb_2O_5 \cdot nH_2O$ can continuously hydrolyze cellobiose to glucose over the reaction time (Figure 6(A)(e)), reaching 5% glucose yield after 6 h. At the same catalyst weight, the activities of porous $Nb_2O_5 \cdot nH_2O$−L64 and −P85 are similar to those of bulk $Nb_2O_5 \cdot nH_2O$, Amberlyst-15, and Nafion NR50, and are larger than that of SAC-13. On the other hand, $Nb_2O_5 \cdot nH_2O$−P103 and −P123 have higher catalytic performance for the reaction than the other tested catalysts. The catalytic performance, acid amount and structural parameters of each catalyst are summarized in Table 4. The turnover frequency (TOF) of bulk $Nb_2O_5 \cdot nH_2O$ is larger than that of Amberlyst-15, Nafion NR50, and SAC-13, because bulk $Nb_2O_5 \cdot nH_2O$ has similar or higher catalytic performance to these conventional SO_3H-bearing polymers, despite a low acid site density. The porous $Nb_2O_5 \cdot nH_2O$ samples had similar or higher glucose yields and TOFs than bulk $Nb_2O_5 \cdot nH_2O$. In particular, the glucose yields of $Nb_2O_5 \cdot nH_2O$−P103 and −P123 were three times larger than that of bulk $Nb_2O_5 \cdot nH_2O$, and the TOF for $Nb_2O_5 \cdot nH_2O$−P103 was 9 times larger than that of bulk $Nb_2O_5 \cdot nH_2O$. $Nb_2O_5 \cdot nH_2O$−P85 shows the smallest glucose yield and TOF among the porous $Nb_2O_5 \cdot nH_2O$ samples. Cellobiose is a large molecule (width, ca. 0.61 nm; length, ca. 1.2 nm), and therefore, the accessibility of cellobiose to Brønsted acid sites is restricted by the relatively narrow pores in $Nb_2O_5 \cdot nH_2O$−P85. $Nb_2O_5 \cdot nH_2O$−L64 has a similar acid density and surface area to $Nb_2O_5 \cdot nH_2O$−P103, and the latter had a large glucose yield and TOF than the former, which indicates that the Brønsted acid sites in $Nb_2O_5 \cdot nH_2O$−P103 with relatively large pores (1.8−8.0 nm) are more accessible to cellobiose than those in $Nb_2O_5 \cdot nH_2O$−L64 (3.4 nm). The highest glucose yield for $Nb_2O_5 \cdot nH_2O$−P123 is due to the large amounts of acid sites and pore size (2−10 nm). However, the TOF is moderate compared with those of $Nb_2O_5 \cdot nH_2O$−L64 and −P103. This suggests that $Nb_2O_5 \cdot nH_2O$−P123 has a smaller amount of effective acid sites than $Nb_2O_5 \cdot nH_2O$−L64 and −P103. Although porous $Nb_2O_5 \cdot nH_2O$ samples have similar or higher activity than bulk $Nb_2O_5 \cdot nH_2O$ for the hydrolysis of cellobiose, this cannot be simply attributed to only the acidity and acid site density.

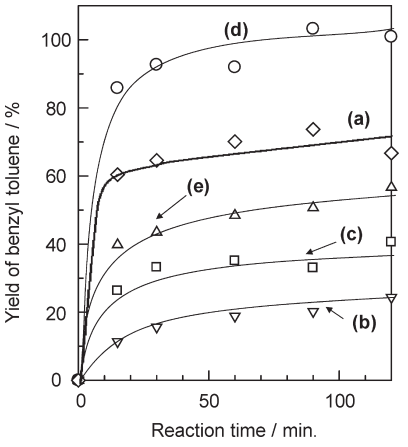

Figure 7. Time courses for benzyltoluene formation by the Friedel−Crafts alkylation of toluene with benzyl chloride over (a) mesoporous $Nb_2O_5 \cdot nH_2O$ prepared with L64, (b) supermicroporous $Nb_2O_5 \cdot nH_2O$ prepared with P85, (c) mesoporous $Nb_2O_5 \cdot nH_2O$ prepared with P103, (d) mesoporous $Nb_2O_5 \cdot nH_2O$ prepared with P123, and (e) bulk $Nb_2O_5 \cdot nH_2O$.

(32) Iizuka, T.; Ogasawara, K.; Tanabe, K. *Bull. Chem. Soc. Jpn.* **1983**, *56*, 2927.
(33) Ragauskas, A. J.; Williams, C. K.; Davison, B. H.; Britovsek, G.; Cairney, J.; Eckert, C. A.; Frederick, W. J.; Hallett, J. P.; Leak, D. J.; Liotta, C. L.; Mielenz, J. R.; Murphy, R.; Templer, R.; Tschaplinski, T. *Science* **2006**, *311*, 484.
(34) Hahn-Haegerdal, B.; Galbe, M.; Gorwa-Grauslund, M. F.; Liden, G.; Zacchi, G. *Trends Biotechnol.* **2006**, *24*, 549.
(35) Corma, A.; Iborra, S.; Velty, A. *Chem. Rev.* **2007**, *107*, 2411.
(36) Harmer, M. A.; Sun, Q. *Appl. Catal., A* **2001**, *221*, 45.
(37) Harmer, M. A.; Farneth, W. E.; Sun, Q. *J. Am. Chem. Soc.* **1996**, *118*, 7708.
(38) Harmer, M. A.; Sun, Q.; Vega, A. J.; Farneth, W. E.; Heidekum, A.; Folderich, W. F. *Green Chem.* **2000**, *1*, 7.

Table 5. Catalytic Activity for the Friedel−Crafts Alkylation of Toluene with Benzyl Chloride and Structural Parameters for Supermicroporous, Mesoporous, and Bulk $Nb_2O_5 \cdot nH_2O$

	surfactant	S_{BET} ($m^2\ g^{-1}$)	pore size (nm)	acid amount (LAS)[a] (mmoL g^{-1})	benzyltoluene yield[b] (mmoL)	TOF[c] (s^{-1})
porous $Nb_2O_5 \cdot nH_2O$	L64	312	3.4	0.19	12.0	0.35
	P85	278	1.6	0.13	2.4	0.10
	P103	246	1.8−8.0	0.14	5.6	0.22
	P123	343	2.0−10.0	0.18	17.4	0.54
bulk $Nb_2O_5 \cdot nH_2O$		171		0.15	8.4	0.31

[a] Estimated by pyridine adsorption experiment. [b] Yield of benzyltoluene for 15 min. [c] Reaction time: 15 min.

There is no significant difference in acidity among the tested porous and bulk $Nb_2O_5 \cdot nH_2O$ samples. Furthermore, $Nb_2O_5 \cdot nH_2O$−P103 with a low acid site density exhibits high catalytic performance. One possible explanation for the high catalytic performance of the porous materials is capillary condensation.[39] Cellobiose can be effectively incorporated into the large-sized mesopores of $Nb_2O_5 \cdot nH_2O$ by capillary action and is then converted into glucose over Brønsted acid sites. Facile diffusion of the reactant and product within the large mesopores would also contribute to the high catalytic performance.

After the reaction for 6 h, the porous samples could be readily separated from reaction solution by simple decantation, and the catalytic activities of the collected samples were examined by the reaction again. The results for the catalyst reuse experiment are summarized in Table S1 in the Supporting Information. In all samples, the catalytic activity of the reused sample is the same as that of the fresh sample. The mesoporous structures of $Nb_2O_5 \cdot nH_2O$ samples before and after the hydrolysis of cellobiose were examined by XRD, SEM, and N_2 adsorption analysis. Table S2 and Figures S1 and S2 in the Supporting Information show the structural parameters and small and wide-angle XRD patterns for the porous $Nb_2O_5 \cdot nH_2O$ samples, respectively, before and after the reaction. There is no significant difference in XRD pattern, BET surface area, pore volume, and pore size between the fresh and reused samples, indicating that in the prepared $Nb_2O_5 \cdot nH_2O$ samples the original mesoporous structure and mesoporosity are stable under the reaction conditions. The SEM images for the samples before and after the reaction (Figure 3 and Figure S3 in the Supporting Information) also support the stability of the porous $Nb_2O_5 \cdot nH_2O$ samples.

The catalytic properties of $Nb_2O_5 \cdot nH_2O$ were also tested by the Friedel−Crafts alkylation of toluene with benzyl chloride, which can proceed only on Lewis acid sites. Friedel−Crafts-type reactions of aromatic compounds are important reactions in both the petroleum and chemical industries.[40] Figure 7 shows time courses for benzyl toluene formation over bulk, supermicroporous, and mesoporous $Nb_2O_5 \cdot nH_2O$. Bulk $Nb_2O_5 \cdot nH_2O$ can progressively produce benzyl toluene over the reaction time, reaching a 50% benzyl toluene yield after 120 min. This reaction cannot proceed in the presence of concentrated sulfuric acid, which suggests that benzyl toluene is formed on the Lewis acid sites of $Nb_2O_5 \cdot nH_2O$. Although mesoporous $Nb_2O_5 \cdot nH_2O$−P123 and −L64 exhibit higher catalytic activity than bulk $Nb_2O_5 \cdot nH_2O$, the catalytic activities for $Nb_2O_5 \cdot nH_2O$−P103 and −P85 are more moderate than that of bulk $Nb_2O_5 \cdot nH_2O$. The structural parameters and catalytic activity of the prepared samples are listed in Table 5. The amount of Lewis acid sites given in the table was estimated from FT-IR measurement with pyridine adsorption.[25−27,41] There was no considerable difference in acid strength and the amount of Lewis acid sites among the tested samples, including bulk $Nb_2O_5 \cdot nH_2O$, nevertheless, the yield and TOF of $Nb_2O_5 \cdot nH_2O$−P85 were smaller than those of the other tested samples. The low catalytic activity of $Nb_2O_5 \cdot nH_2O$−P85 is again attributed to narrow pore size. All of the tested samples, except for $Nb_2O_5 \cdot nH_2O$−P85, have similar TOF, which implies that large mesopores are not so advantageous for the Friedel−Crafts alkylation of toluene with benzyl chloride, in contrast to the hydrolysis of cellobiose. This difference may be attributed to the hydrophobic−hydrophilic properties of the reactants. Mesoporous, supermicroporous, and bulk $Nb_2O_5 \cdot nH_2O$ samples possess not only acidic OH groups as Brønsted acid sites, but also high densities of neutral OH groups, and the amount of neutral OH groups is much (several times) larger than that of acidic OH groups.[20,32] Such hydrophilic mesopores would facilitate the incorporation and access to catalytic active sites by hydrophilic reactants such as cellobiose, but would not be significantly advantageous for hydrophobic reactants such as toluene and benzyl chloride.

Conclusion

Mesoporous $Nb_2O_5 \cdot nH_2O$ was successfully prepared using amphiphilic block copolymers (L64, P103, and P123) as structure-directing templates. FT-IR analyses using CO as a basic probe molecule indicated that the acid strength of both Lewis and Brønsted acid site for mesoporous and supermicroporous $Nb_2O_5 \cdot nH_2O$ are identical to that for bulk $Nb_2O_5 \cdot nH_2O$. Although mesoporous $Nb_2O_5 \cdot nH_2O$ with large pores exhibits higher catalytic performance for the hydrolysis of cellobiose (a hydrophilic reaction) than bulk $Nb_2O_5 \cdot nH_2O$ because of facile incorporation and diffusion of the hydrophilic reactants in the hydrophilic mesopores, this is not advantageous for

(39) Corma, A. *Chem. Rev.* **1997**, *97*, 2373.
(40) Sartori, G.; Maggi, R. *Chem. Rev.* **2006**, *106*, 1077.
(41) Hughes, T. R.; White, H. M. *J. Phys. Chem.* **1967**, *71*, 2192.

the Friedel−Crafts alkylation of toluene with benzyl chloride (a hydrophobic reaction).

Acknowledgment. This work was supported by the New Energy and Industrial Technology Development Organization (NEDO, 04A32502), and the Research and Development in a New Interdisciplinary Field Based on Nanotechnology and Materials Science programs of the Ministry of Education, Culture, Sports, Science and Technology (MEXT) of Japan.

Supporting Information Available: Additional tables and figures (PDF). This material is available free of charge via the Internet at http://pubs.acs.org.